Published in final edited form as:
J Xray Sci Technol. 2014 January 1; 22(3): 321–334. doi:10.3233/XST-140428.

Image quality and dose efficiency of high energy phase sensitive x-ray imaging: Phantom studies

Molly Donovan Wong[a], **Xizeng Wu**[b], and **Hong Liu**[a,*]

[a]Center for Bioengineering and School of Electrical and Computer Engineering, University of Oklahoma, Norman, OK, USA

[b]Department of Radiology, University of Alabama at Birmingham, Birmingham, AK, USA

Abstract

The goal of this preliminary study was to perform an image quality comparison of high energy phase sensitive imaging with low energy conventional imaging at similar radiation doses. The comparison was performed with the following phantoms: American College of Radiology (ACR), contrast-detail (CD), acrylic edge and tissue-equivalent. Visual comparison of the phantom images indicated comparable or improved image quality for all phantoms. Quantitative comparisons were performed through ACR and CD observer studies, both of which indicated higher image quality in the high energy phase sensitive images. The results of this study demonstrate the ability of high energy phase sensitive imaging to overcome existing challenges with the clinical implementation of phase contrast imaging and improve the image quality for a similar radiation dose as compared to conventional imaging near typical mammography energies. In addition, the results illustrate the capability of phase sensitive imaging to sustain the image quality improvement at high x-ray energies and for – breast – simulating phantoms, both of which indicate the potential to benefit fields such as mammography. Future studies will continue to investigate the potential for dose reduction and image quality improvement provided by high energy phase sensitive contrast imaging.

Keywords

Phase contrast x-ray imaging; phase sensitive x-ray imaging; phase retrieval; average glandular dose; ACR; contrast-detail

1. Introduction

Mammography is the most widely used diagnostic technique for breast cancer detection [1], and clinical trials have proven its ability to decrease mortality rates [2–7]. The technology has evolved since the development of dedicated mammography systems began in the 1950s [8] with a consistent goal of balancing the need for adequate image quality to allow early detection of breast cancer with minimizing patient dose to reduce the risk of harmful

*Corresponding author: Center for Bioengineering and School of Electrical and Computer Engineering, University of Oklahoma, 110 West Boyd Street, Devon Energy Hall 150, Norman, OK 73019, USA. Tel.: +1 405 325 4286; Fax: +1 405 325 7066; liu@ou.edu..

radiation. However, the mechanism by which x-ray images are formed, which relies solely on attenuation contrast, has remained the same. The similar composition between normal and malignant breast tissue [9–11] produces very low attenuation contrast, which presents a significant challenge for early cancer detection. Improving the image quality in conventional x-ray imaging can only be accomplished a few ways: lowering the x-ray energy to increase the amount of radiation absorbed by the tissue [9,11,12], and utilizing an anti-scatter grid between the object and detector to reduce the image degradation caused by scattered x-rays [9,13]. Both methods improve the signal-to-noise ratio, and thus the image quality, of the image; however, this is accomplished at the expense of an increased radiation dose to the patient. Thus, balancing the tradeoff between image quality and radiation dose remains a significant challenge to the field of mammography.

An emerging technology called phase contrast imaging has the potential to improve this tradeoff. Phase contrast imaging is based on the property of x-rays as electromagnetic waves, which therefore also experience phase changes when passing through objects, resulting in image contrast produced by both refraction and attenuation effects [11,14–19]. Theoretical comparisons for given types of tissue indicate that the refraction amounts are much larger than the attenuation amounts [15,20–22]. The technology utilizes a similar configuration to conventional x-ray imaging, with the addition of an air gap between the object and the detector, as well as a microfocus source emitting polychromatic x-rays, which is readily available and clinically acceptable [17–19]. Thus phase contrast imaging has received significant research focus, and numerous studies have indicated the potential of the new technology to benefit mammography. Numerous studies have reported improved image quality [10,11,14,16–18,20,21,23–25] and sustained image quality improvement with increasing thickness [11,14,16–18,20,24,25], which may be applicable to improving mammography. The introduction of the air gap transforms the phase gradients generated by the interference of x-rays with different phase shifts into intensity gradients on the image, which combine with the attenuation contrast to produce enhanced edges along the boundaries between structures [11,12,15,16,20,25]. However, the bulk of the phase contrast in a given tissue area may be lost if the phase shifts vary slowly. This occurs because phase contrast is proportional to the Laplacian and gradient differentials of the phase shifts. In order to fully exhibit tissue phase contrast, one needs to disentangle tissue phase shifts from the combined attenuation and phase contrast in a phase sensitive projection. The procedure of retrieving phase shift maps from a phase sensitive projection is called phase retrieval, and the commonly used approaches require the acquisition of multiple images with varying object-detector distances per angular projection [26–32]. Unfortunately, this is time-consuming and results in a high radiation dose. We have observed that soft tissue attenuation cross sections are very well approximated by that of incoherent scattering for x-rays from approximately 60 keV to 500 keV [33]. Within this x-ray energy range, we found that both x-ray attenuation and phase-shift in soft tissue are determined by the projected tissue electron density $\rho_{e,p} = \int \rho_e(s)ds$, which is an integral of tissue electron densities (ρ_e) over the ray path. We call this observation the phase attenuation duality (PAD), and we developed a robust and low-dose phase retrieval method called the PAD-based phase retrieval method, which requires only a single phase contrast projection image to retrieve the phase map of the sample [29,30].

Phase sensitive imaging has the potential to decrease the radiation dose to the patient, due to the air gap providing a comparable amount of scatter rejection and resultant image quality improvement as the grid used in conventional imaging without the dose increase [10,16,23], as well as the fact that the phase contrast effect decreases much more slowly than attenuation with increasing x-ray energy [10,12,14, 15,34,35]. Therefore, the x-ray energy can potentially be increased without compromising the image quality. This would provide further dose reduction, as high energy x-rays are much more penetrating to the breast. Increasing the x-ray energy also has the potential to overcome an existing challenge in phase contrast imaging involving the number of output quanta generated with the microfocus source. The number of quanta N generated for a given distance from the focal spot is represented as follows [9]:

$$N \propto kV^2 \cdot mAs, \quad (1)$$

where kV represents the x-ray energy and mAs indicates a quantity representing the tube current in units of milliamperes (mA) multiplied by the exposure time in units of seconds (s). Microfocus sources produce limited tube current as compared to conventional sources, due to the smaller focal spot size. For the same x-ray energy and exposure time, a reduction in tube current reduces the x-ray quanta output proportionately. Therefore, the exposure time must be increased by the same proportion when utilizing the same x-ray energy, in order to balance the reduced number of x-ray quanta [10,18,20]. However, increasing the x-ray energy instead of the exposure time only requires an increase by the square root of the proportion. Therefore, phase sensitive imaging at high energies holds the potential to produce the same number of x-ray quanta at clinical exposure times, which is an indication of the clinical feasibility and the ability to benefit the field of mammography.

The primary goal of this preliminary study was to compare the image quality provided by phase sensitive images at 100 kV to conventional images at 40 kV, in an effort to determine the potential of high energy phase sensitive imaging to increase the image quality at a similar radiation dose. Typical mammography energies are between approximately 25 and 33 kV, but 40 kV is the lowest energy output by the x-ray tube utilized in this study. To the best of our knowledge, the comparison of high energy phase contrast imaging with low energy conventional images has not been reported previously, with the exception of our introductory study [36].

2. Materials and methods

2.1. System and measurement components

As illustrated in Fig. 1, the inline x-ray imaging system prototype utilized in this study consists of the imaging and measurement components mounted along an optical rail, which allows the use of a precise laser alignment process detailed in a previous study [37]. This also provides the ability to adjust the x-ray source-to-object ($R1$) and object-to-detector ($R2$) distances to facilitate acquisition of images in both phase contrast and conventional imaging modes. The configuration for acquiring the phase contrast images is given in Fig. 1(a). The source-to-detector distance ($R1$ + $R2$) was 182.88 cm. A magnification factor of 2.5 was utilized for this study, which corresponds to a source-to-object distance (*R*1) of 73.15 cm, according to the following formula [9,38]:

$$M=\frac{R1+R2}{R1}. \quad (2)$$

Following the acquisition of the images, phase retrieval was performed as detailed in previous studies [29–32]. Next, Fig. 1(b) demonstrates the conventional image configuration, which requires the object to be placed directly in contact with the detector, resulting in an *R*2 value of zero and a magnification factor of 1. Comparison images were acquired with the same *R*1 value as the phase contrast images to facilitate comparison with similar source-to-object distances.

The microfocus x-ray source (Model L8121-03, Hamamatsu Photonics, Japan) used in this study consists of a tungsten target and a 200 μm thick Beryllium output window with adjustable tube current and voltage ranging from 40 to 150 kV. The distance from the focal spot to the output window is 17 mm, and the diameter of the focal spot is 7 μm for tube operation at an output power of 10 W. The settings utilized in this study were 40 kVp, 250 μA for the conventional images and 100 kVp, 100 μA for the phase contrast images. Our prototype phase contrast x-ray imaging system incorporates a computed radiography detection system with mammography plates (Regius 190, Konica Minolta Medical Imaging, Wayne, New Jersey). The imaging size of the plates used in the experiments was 24 by 30 cm, and the system provides a pixel pitch of 43.75 μm. A challenge in this study involves the utilization of mammography plates for much higher energies than designed for the phase sensitive images, resulting in decreased quantum efficiency. However, the use of general radiography plates would reduce the spatial resolution, as they only provide a pixel pitch of 87.5 μm. The resulting tradeoff in the type of plate utilized will be an interesting topic evaluated in a future study. Standard flat fielding procedures [9] were performed to all images acquired in the study. Window/level adjustments were also performed for optimal viewing.

2.2. Dose calculation

Breast cancer typically arises in the glandular tissue [9,39]; therefore, the average glandular dose has been established as the standard measurement of radiation dose in mammography, and guidelines have been created by numerous national and international councils for its calculation and supervision in clinical environments [39–43]. The formula for calculation of the average glandular dose D_g is as follows [9,44,45]:

$$D_g=D_{gN}\cdot X_{ESE}, \quad (3)$$

where D_{gN} is the normalized average glandular dose coefficient and X_{ESE} is the object entrance exposure. The measurements of object entrance exposure were obtained with a calibrated ionization chamber (10X9-180 ionization chamber, Model 9095 measurement system, Radcal Corporation, Monrovia, California). Five measurements at each mode were acquired in an effort to reduce the error in the measurements. The entrance exposure at exactly the same location as the object was measured for both phase contrast and conventional modes. D_{gN} is determined by experimental and computer simulation methods based on the following factors: radiation quality (x-ray energy or half value layer), x-ray tube target material, filter material, breast thickness and breast tissue composition [9]. Due to the complicated nature of the calculations, as well as the small range of values in mammography for each of the D_{gN} calculation parameters, numerous studies have published tables of D_{gN} values that are widely used in clinical and research environments [44–49]. However, the values must typically be calculated directly in investigational studies, due to the use of parameters outside the standard values. This study therefore applied a Monte Carlo simulation process described previously [45,48,49] to estimate the D_{gN} values for each mode. The simulations assumed the presence of an object with 50% adipose and 50% glandular tissue composition in the path of the x-ray beam. To accomplish similar radiation doses among the phase contrast and conventional images, a target D_g amount of 200 mrad was selected, and the corresponding target object entrance exposure amount was determined for each mode based on the calculated D_{gN} value. The exposure time delivering the target object entrance exposure amount for each mode was then determined. Table 1 provides the D_{gN}, X_{ESE}, and exposure time values for each mode, both of which deliver a D_g value of approximately 200 mrad.

2.3. Phantoms

Several phantoms were utilized in this study to provide a comprehensive image quality evaluation. First, the evaluation of system performance based on standard mammography quality control procedures, including the American College of Radiology (ACR) phantom, has been established as a widely-accepted quantitative comparison method [11,23,25,35]. Thus, a standard 4.5 cm thick ACR phantom (Model K-598, Nuclear Associates, Carle Place, New York, USA) was utilized in this study. Each image was scored according to the number of distinguishable test objects, as outlined in the mammography quality control manual [50], which separates the ACR test objects into groups of fibers, specks and masses. Following these guidelines, separate scores can be determined for each of the groups, and the scores are added together to achieve the overall image score, which provides a quantitative comparison of the relative image quality provided by the high energy phase sensitive and low energy conventional images. To analyze the images, they were randomly presented to a group of 8 observers. Each observer completed the analysis independently, utilizing the same monitor and viewing conditions. The observers could adjust the window and level settings, as well as the magnification and rotation of the images, to suit their viewing preferences. The results were then averaged to determine individual scores for fibers, specks and masses, as well as an overall combination score for each of the comparison images.

Next, a contrast-detail (CD) phantom was utilized to provide an additional level of comparison. Contrast-detail analysis has also been widely accepted as a simple and effective method for comparison of medical imaging systems or techniques [51–56]. CD phantoms typically consist of a matrix of circles with varying diameters along one axis to represent object size, and varying thicknesses along the other axis to produce contrast within the image [9,38]. The 1 cm thick CD phantom utilized in this study (Model 083, CIRS, Norfolk, Virginia, USA) consists of seven rows ranging in diameter from 1.5 to 4.5 mm, and seven columns ranging in thickness from 0.25 to 4.5 mm. The analysis involves an observer identifying the minimum perceptible thickness in the image for each diameter. The results are compiled into a contrast-detail curve indicating the contrast required to distinguish an object as a function of the object size, which illustrates the resolving power of the system or technique. Thus curves for different systems or techniques can easily be compared, as a system exhibiting higher performance produces a contrast-detail curve located closer to the x-y axis. In this study, the comparison images were randomly presented to 8 observers for contrast-detail analysis, and the study was performed exactly as detailed for the ACR observer study. The observer results were averaged and represented on a contrast-detail curve illustrating the threshold contrast (represented by the minimum perceptible disk thickness) as a function of the disk diameter. The Student t distribution is frequently utilized in research environments for analyzing collected data, due to its proven ability to construct accurate confidence intervals on smaller data sets with unknown variance [57–59]. As typically applied in comparisons, this study utilized a 95% confidence interval with $n - 1$ degrees of freedom, where n represents the number of observers.

Next, a 1.5 mm thick acrylic edge phantom was employed to illustrate the overshooting effects provided as the result of the edge enhancement in phase-contrast images [11,12,15,16,20,35]. Acrylic edge phantoms images not only provide a visual indication of the edge enhancement, but they can also be utilized to determine edge profiles that serve as a graphical indication of the edge enhancement [11,18,35]. An edge profile illustrates the intensity values along a line perpendicular to the edge, which indicates the edge enhancement in the phase contrast images through an overshooting effect along the edge transition.

Finally, significant research focus has also been dedicated to the image quality provided by phase contrast with breast specimens [10,14,24,25] for qualitative investigation of the clinical potential of a system or technique. However, due to the difficulty of utilizing human specimens in research environments, phantoms are typically utilized to simulate human tissue. In this study, a new phantom providing tissue-equivalent x-ray images was utilized. The Mammography BR3D phantom (Model 020, CIRS, Norfolk, Virginia, USA) was fabricated from materials simulating 100% adipose and glandular tissues blended together in an approximate 50/50 ratio by weight, which produces a tissue-equivalent heterogeneous background on an x-ray image [60]. The phantom consists of a set of five pieces of the same size, each having a thickness of 10 mm and a different blend of the materials. The combination of the five layers was designed to produce realistic tissue-equivalent x-ray images, and the 5 cm thickness provides an additional level of comparison involving the object thickness, the importance of which to mammography was detailed previously.

3. Results and discussion

3.1. ACR phantom

The ACR phantom image produced by performing phase retrieval on the high energy phase contrast image is provided in Fig. 2(a), while the low energy conventional image is provided in Fig. 2(b). The images exhibit very similar image quality, with slightly higher contrast demonstrated by the phase retrieved image. This indicates the capability of phase contrast imaging at higher energies to meet or exceed the existing image quality standards designed for low energy attenuation contrast imaging. The averaged observer study scores for each individual object type, as well as the total score, are provided in Fig. 3. The results reinforce the visual indication of comparable image quality. It is also interesting to note the higher scores achieved by the phase contrast images in the specks category. The ability to distinguish the smallest test objects more clearly is an indication of the improvement in image quality provided by phase contrast imaging.

3.2. Contrast-detail phantom

The contrast-detail phantom image produced by performing phase retrieval on the high energy phase contrast image is provided in Fig. 4(a), while the low energy conventional image is provided in Fig. 4(b). Visual comparison reveals enhanced image quality in the phase contrast image through increased contrast. The number of test objects distinguished is comparable between the images, once again an indication of the capability of high energy phase contrast imaging to meet or exceed the existing image quality standards designed for low energy attenuation contrast imaging. In addition, the edge enhancement delivered by phase contrast imaging is clearly demonstrated through the white circles highlighting the edges of the test objects.

The observer study was performed to provide a quantitative comparison of the two images, and the corresponding averaged contrast-detail curves are provided in Fig. 5. As detailed previously, superior image quality is demonstrated by a curve closer to the x-y axis. The phase contrast curve is closer to the axis for all points, with the exception of the diameter of 2.5 mm. For that point, the results for both images were within the Student *t* error bars, indicating no statistically significant difference between the two values. However, the phase retrieval results are outside the Student *t* error bars for the rest of the data points, which indicates that the phase retrieval image results are superior to the conventional image results. It is interesting that one point could generate such drastically different results. A possible explanation for this is an imperfection in the phantom or the image which prevented the observers from scoring it consistently.

3.3. Acrylic edge phantom

The acrylic edge phantom images acquired by the high energy phase contrast and low energy conventional modes are provided in Fig. 6(a) and (b), respectively. The edge is more clearly distinguished in the phase contrast image as compared to the conventional image, indicating the edge enhancement provided by phase contrast. In addition, the phase contrast overshooting effect is demonstrated in Fig. 6(a) through the white line highlighting the edge. As a second demonstration of the phase contrast effect, edge profiles for the phase contrast and conventional modes are provided for comparison in Fig. 7(a) and (b), respectively. The edge profiles have been normalized to facilitate effective comparison. In contrast to the conventional image, the phase contrast image exhibits overshooting along the edge transition, which is a graphical indication of the edge enhancement illustrated in Fig. 6(a).

3.4. Tissue-equivalent phantom

The tissue-equivalent phantom images acquired by high energy phase contrast and low energy conventional imaging are provided in Fig. 8(a) and (b), respectively. As detailed previously, the tissue-equivalent phantom was designed to simulate a human breast, through not only the tissue composition but also the phantom thickness, the results of which are both of great importance in this study investigating the clinical feasibility of high energy phase contrast imaging for mammography. Although the phantom images are an interesting simulation of a human breast, they clearly indicate the potential of the technology in both respects. The phase contrast effect is evident in the image, through not only the edge enhancement, but also the ability to distinguish fine features within the images. Since the phase contrast effect decreases with increasing x-ray energy, the image quality demonstrated in the high energy phase contrast image is encouraging. In addition, the difference between the phase contrast and conventional images is clearly demonstrated in the lower contrast of the structures within the conventional image. The comparison indicates the image quality enhancement provided by phase contrast imaging in comparison to conventional imaging, as well as the ability to sustain the improvement at high energies and for clinical thicknesses.

As mentioned previously, a challenge in this study involved the use of mammography CR plates for the high energy images, which results in much lower quantum efficiency. Thus the image quality difference between the high energy phase contrast and low energy conventional images could be much more pronounced if the quantum efficiency were improved. Future studies will evaluate the tradeoff between the quantum efficiency and spatial resolution presented by the use of mammography versus general radiography CR plates, in a continued effort to investigate the potential for dose reduction and image quality improvement provided by high energy phase contrast imaging. A different detection system providing higher spatial resolution for higher x-ray energies, such as a Hamamatsu CMOS imaging sensor, could also be utilized for comparison image acquisition.

Another factor affecting the comparison in this study involves the lack of a grid for the conventional images, which could have provided scatter reduction for the images. However, as mentioned previously, the grid drastically increases the radiation dose, thus any benefits of the scatter reduction likely would have been offset by the resultant dose increase.

4. Conclusion

The primary goal of this preliminary study was to compare the image quality provided by high energy phase sensitive images with conventional images at near typical mammography energies, in an effort to determine the potential of high energy phase sensitive imaging to increase the image quality at a similar radiation dose. To accomplish this, an image quality evaluation consisting of the following phantoms was performed: ACR, CD, acrylic edge and tissue-equivalent. High energy phase contrast and low energy conventional images of each phantom were acquired with similar absorbed radiation doses for investigation of the relative image quality. Direct comparison of the phantom images indicated comparable or improved image quality for all phantoms. Quantitative comparisons were performed through ACR and CD observer studies consisting of 8 observers, both of which indicated higher image quality in the phase contrast images.

The results of this study demonstrate the ability of high energy phase sensitive imaging to overcome existing challenges with the clinical implementation of phase contrast imaging and improve the image quality for a similar radiation dose as compared to conventional imaging near typical mammography energies. In addition, the results illustrate the capability of phase sensitive imaging to sustain the image quality improvement at high x-ray energies and for clinical thicknesses, both of which indicate the potential to benefit fields such as mammography. Future studies will continue to investigate the potential for dose reduction and image quality improvement provided by high energy phase sensitive contrast imaging, through conducting phantom studies including human tissue samples as well as observer studies with more participants. In addition, a comprehensive comparison to conventional imaging with clinical mammography equipment will be performed. Finally, this technique can be combined with numerous recent advancements in phase contrast imaging and radiation dose reduction for further potential benefit to the field of medical x-ray imaging [61–63].

Acknowledgments

The authors gratefully acknowledge the support of a DoD Breast Cancer research grant (W81XWH-08-1-0613), as well as an NIH grant (1R01CA142587), and a grant from the University of Oklahoma Charles and Peggy Stephenson Cancer Center funded by the Oklahoma Tobacco Settlement Endowment Trust. The authors would like to acknowledge the support of the Charles and Jean Smith Chair endowment fund as well.

References

[1]. Karellas A, Vedantham S. Breast cancer imaging: A perspective for the next decade. Medical Physics. 2008; 35:4878–4897. [PubMed: 19070222]

[2]. Hendrick RE, Smith RA, Rutledge JH III, Smart CR. Benefit of screening mammography in women aged 40–49: A new meta-analysis of randomized controlled trials. J Natl Cancer Inst Monogr. 1997; 22:87–92. [PubMed: 9709282]

[3]. Moss S. A trial to study the effect on breast cancer mortality of annual mammographic screening in women starting at age 40. J Med Screen. 1999; 6:144–148. [PubMed: 10572845]

[4]. Shapiro S, Venet P. Strax and L. Periodic breast cancer screening in reducing mortality from breast cancer. Journal of American Medical Association. 1971; 215:1775–1785.

[5]. Shapiro S. Periodic screening for breast cancer: The HIP Randomized Controlled Trial. J Natl Cancer Inst Monogr. 1997; 1997:27–30. [PubMed: 9709271]

[6]. Tabár L, Vitak B, Chen H, Yen M, Duffy S, Smith R. Beyond randomized controlled trials: Organized mammo-graphic screening substantially reduces breast carcinoma mortality. Cancer. 2001; 91:1724–1731. [PubMed: 11335897]

[7]. Thurfjell EL, Lindgren JA. Breast cancer survival rates with mammographic screening: similar favorable survival rates for women younger and those older than 50 years. Radiology. Nov 1.1996 201:421–426. [PubMed: 8888234]

[8]. Bassett L, Gold R. The evolution of mammography. American Journal of Roentgenology. 1988; 150:493–498. [PubMed: 3277343]

[9]. Bushberg, J.; Seibert, J.; Leidholdt, E., Jr.; Boone, J. The Essential Physics of Medical Imaging. Second ed.. Lippincott Williams & Wilkins; Philadephia, Pennsylvania: 2002.

[10]. Ingal V. Phase mammography – A new technique for breast investigation. Physics in Medicine and Biology. 1998; 43:2555–2567. [PubMed: 9755945]

[11]. Kotre C, Birch I. Phase contrast enhancement of x-ray mammography: A design study. Physics in Medicine and Biology. 1999; 44:2853–2866. [PubMed: 10588289]

[12]. Monnin P, Hoszowska J, Valley J, Meuli R, Verdun F. Quantitative characterization of edge enhancement in phase contrast x-ray imaging. Medical Physics. 2004; 31:1372–1383. [PubMed: 15259641]

[13]. Law J. The development of mammography. Physics in Medicine and Biology. 2006; 51:155–167.

[14]. Arfelli F, et al. Low-dose phase contrast x-ray medical imaging. Physics in Medicine and Biology. Oct.1998 43:2845–2852. [PubMed: 9814522]

[15]. Fitzgerald R. Phase-sensitive x-ray imaging. Physics Today. 2000; 53:23–26.

[16]. Matsuo S, Katafuchi T, Tohyama K, Morishita J, Yamada K, Fujita H. Evaluation of edge effect due to phase contrast imaging for mammography. Medical Physics. 2005; 32:2690–2697. [PubMed: 16193800]

[17]. Pogany A, Gao D, Wilkins S. Contrast and resolution in imaging with a microfocus x-ray source. Review of Scientific Instruments. 1997; 68:2774–2782.

[18]. Wilkins S, Gureyev T, Gao D, Pogany A, Stevenson A. Phase-contrast imaging using polychromatic hard x-rays. Nature. 1996; 384:335–338.

[19]. Wu X, Liu H. Clinical implementation of x-ray phase-contrast imaging: theoretical foundations and design considerations. Medical Physics. 2003; 30:2169–2179. [PubMed: 12945983]

[20]. Donnelly E, Price R, Pickens D. Quantification of the effect of system and object parameters on edge enhancement in phase-contrast radiography. Medical Physics. 2003; 30:2888–2896. [PubMed: 14655935]

[21]. Momose A, Fukuda J. Phase-contrast radiographs of non-stained rat cerebellar specimen. Medical Physics. 1995; 22:375–379. [PubMed: 7609717]

[22]. Wu X, Liu H. A general theoretical formalism for x-ray phase contrast imaging. Journal of X-Ray Science and Technology. 2003; 11:33–42. [PubMed: 22388096]

[23]. Freedman M, Lo S, Honda C, Makariou E, Sisney G, Pien E, Ohara H, Ishisaka A, Shimada F. Phase contrast digital mammography using molybdenum x-ray: clinical implications in detectability improvement. SPIE. 2003; 5030:533–540.

[24]. Tanaka T, et al. The first trial of phase contrast imaging for digital full-field mammography using a practical molybdenum X-ray tube. Investigative Radiology. Jul.2005 40:385–396. [PubMed: 15973129]

[25]. Zhang D, Donovan M, Fajardo L, Archer A, Wu X, Liu H. Preliminary feasibility study of an in-line phase contrast x-ray imaging prototype. IEEE Transactions on Biomedical Engineering. 2008; 55:2249–2257. [PubMed: 18713694]

[26]. Cloetens P, et al. Quantitative phase tomography of Arabidopsis seeds reveals intercellular void network. Proceedings of the National Academy of Sciences. 2006; 103:14626–14630.

[27]. Nugent KA, et al. Quantitative Phase Imaging Using Hard X Rays. Physical Review Letters. 1996; 77:2961–2964. [PubMed: 10062096]

[28]. Wu X, Liu H. X-Ray cone-beam phase tomography formulas based on phase-attenuation duality. Optics Express. 2005; 13:6000–6014. [PubMed: 19498608]

[29]. Wu X, et al. X-ray phase-attenuation duality and phase retrieval. Optics Letters. 2005; 30:379–381. [PubMed: 15762434]

[30]. Wu X, Yan A. Phase retrieval from one single phase contrast x-ray image. Optics Express. 2009; 17:11187–11196. [PubMed: 19550519]

[31]. Yan A, et al. An attenuation-partition based iterative phase retrieval algorithm for in-line phase-contrast imaging. Optics Express. 2008; 16:13330–13341. [PubMed: 18711570]

[32]. Yan A, et al. Performance analysis of the attenuation-partition based iterative phase retrieval algorithm for in-line phase-contrast imaging. Optics Express. 2010; 18:16074–16089. [PubMed: 20720992]

[33]. Dyson NA. X-rays in Atomic and Nuclear Physics: Longman. 1973

[34]. Donnelly E, Price R. Quantification of the effect of kVp on edge-enhancement index in phase-contrast radiography. Medical Physics. 2002; 29:999–1002. [PubMed: 12094995]

[35]. Zhou Y, Pew H, Rong J, Chen W, Fajardo L, Wu X, Liu H. Phantom imaging with a prototype phase contrast radiography system. SPIE. 2006; 6163:61630E.

[36]. Wong M, Wu X, Liu H. Image quality comparison of high energy phase contrast x-ray images with low energy conventional images: phantom studies. SPIE Proceedings on Dynamics and Fluctuations in Biomedical Photonics VII. 2010; 7563:9.

[37]. Zhang D, Wong M, Wu X, Liu H. A convenient alignment approach for x-ray imaging experiments based on laser positioning devices. Medical Physics. 2008; 35:4907–4910. [PubMed: 19070224]

[38]. Hasegawa, B. Madison. Medical Physics Publishing Corporation; Wisconsin: 1990. The Physics of Medical X-Ray Imaging.

[39]. American College of Radiology. Mammography Quality Control Manual, ACR. 1994.

[40]. American Association of Physicists in Medicine. Equipment requirements and quality control for mammography. 1990. AAPM Report 29

[41]. Institute of Physical Sciences in Medicine. The Commissioning and Routine Testing of Mammographic X-Ray Systems. 1989. IPSM Group Report 59

[42]. International Commission on Radiological Protection. Managing patient dose in digital radiology. 2003. ICRP Report 93

[43]. National Council on Radiation Protection and Measurements. Mammography – a user's guide. 1986. p. 40-48.NCRP Report Number 85

[44]. Boone J. Glandular Breast Dose for Monoenergetic and High-Energy X-ray Beams: Monte Carlo Assessment. Radiology. 1999; 213:23–37. [PubMed: 10540637]

[45]. Wu X, Gingold E, Barnes G, Tucker D. Normalized Average Glandular Dose in Molybdenum Target-Rhodium Filter and Rhodium Target-Rhodium Filter Mammography. Radiology. 1994; 193:83–89. [PubMed: 8090926]

[46]. Dance DR. Monte Carlo calculation of conversion factors for the estimation of mean glandular breast dose. Physics in Medicine and Biology. 1990; 35:1211–1219. [PubMed: 2236205]

[47]. Hendrick RE. Standardization of image quality and radiation dose in mammography. Radiology. 1990; 174:648–654. [PubMed: 2305044]

[48]. Wu X, Barnes G, Tucker D. Spectral dependence of glandular tissue dose in screen-film mammography. Radiology. 1991; 179:143–148. [PubMed: 2006265]

[49]. Wu X. Breast Dosimetry in Screen Film Mammography. Screen Film Mammography: Imaging Considerations and Medical Physics Responsibilities. 1991:159–175.

[50]. Hendrick R, Bassett L, Botsco M, Butler P, Dodd G, Feig S, Gray J, Haus A, Harvey M, Heinlein R, Holland R, Kitts E Jr. McLelland R, McCrohan J, Rossi R, Sullivan D. Mammography Quality Control Manual. American College of Radiology. 1994:43–51.

[51]. Aufrichtig R. Comparison of low contrast detectability between a digital amorphous silicon and a screen-film based imaging system for thoracic radiography. Medical Physics. 1999; 26:1349–1358. [PubMed: 10435537]

[52]. Donovan M, Zhang D, Chen W, Liu H. The characterization of a phase contrast x-ray imaging prototype. SPIE. 2007; 6436:9.

[53]. Liu H, Fajardo L, Barrett J, Baxter R. Contrast-detail detectability analysis: comparison of a digital spot mammography system and an analog screen-film mammography system. Academic Radiology. 1997; 4:197–203. [PubMed: 9084777]

[54]. Pogue B, Willscher C, McBride T, Osterberg U, Paulsen K. Contrast-detail analysis for detection and characterization with near-infrared tomography. Medical Physics. Dec.2000 27:2693–2700. [PubMed: 11190952]

[55]. Rong X, Shaw C, Liu X, Thompson M. Lemacks and S. Comparison of an amorphous silicon/cesium iodide flat-panel digital chest radiography system with screen/film and computed radiography systems – a contrast-detail phantom study. Medical Physics. Nov.2001 28:2328–2335. [PubMed: 11764040]

[56]. Zhang Q, Li Y, Steele B, Wu X, Chen W, Rong J, Liu H. Comparison of a CMOS-based and a CCD-based digital x-ray imaging system: observer studies. Journal of Electronic Imaging. 2005; 14:23002. 6 pages.

[57]. Larsen, R.; Marx, M. An Introduction to Mathematical Statistics and Its Applications. Fourth ed.. Pearson Prentice Hall; Upper Saddle River, NJ: 2006.

[58]. Mendenhall, W.; Sincich, T. Statistics for Engineering and the Sciences. 5th Edition ed.. Prentice Hall; Upper Saddle River, New Jersey: 2007.

[59]. Papoulis, A.; Pillai, S. Probability, Random Variables and Stochastic Processes. Fourth Edition ed.. McGraw-Hill; New York City, New York: 2002.

[60]. CIRS. Mammography BR3D Phantom Manual. CIRS Tissue Simulation and Phantom Technology. 2009.

[61]. Miao H, Wu X, Zhao H, Liu H. A phantom-based calibration method for digital x-ray tomosynthesis. Journal of X-Ray Science and Technology. 2012; 20:17–29. [PubMed: 22398585]

[62]. Wang Z, et al. Low dose reconstruction algorithm for differential phase contrast imaging. Journal of X-Ray Science and Technology. 2011; 19:403–415. [PubMed: 21876288]

[63]. Wong M, Wu X, Liu H. The effects of x-ray beam hardening on detective quantum efficiency and radiation dose. Journal of X-Ray Science and Technology. 2011; 19:509–519.

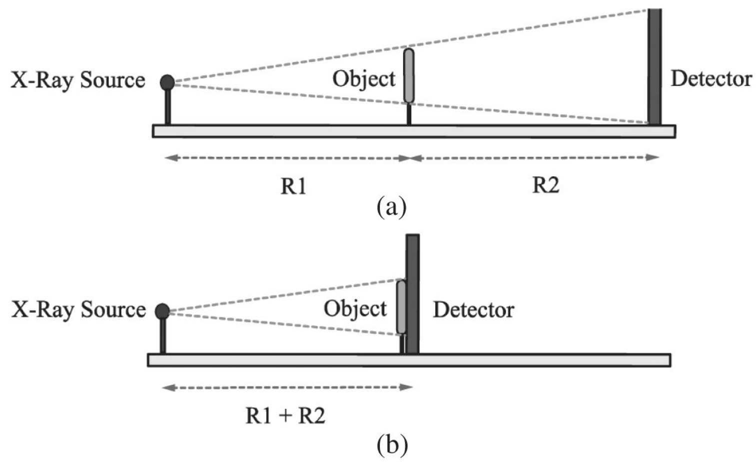

Fig. 1.

The system configurations utilized in this study for: (a) phase contrast images, in which R1 was adjusted to deliver a magnification factor of 2.5, and (b) conventional comparison images, in which the object was placed in contact with the detector. The same R1 value was utilized to facilitate comparison of conventional and phase contrast images with the same source-to-object distance.

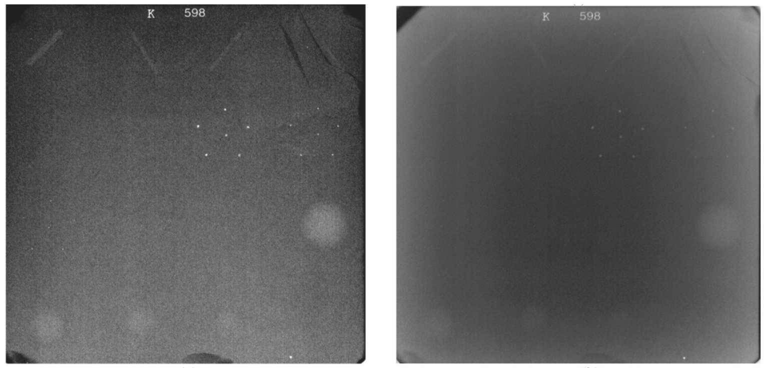

(a) (b)

Fig. 2.

Comparison of ACR phantom images, which were acquired under the following experimental settings: (a) 100 kV, 100 μA and 72 s in phase contrast mode, and (b) 40 kV, 250 μA and 192 s in conventional mode.

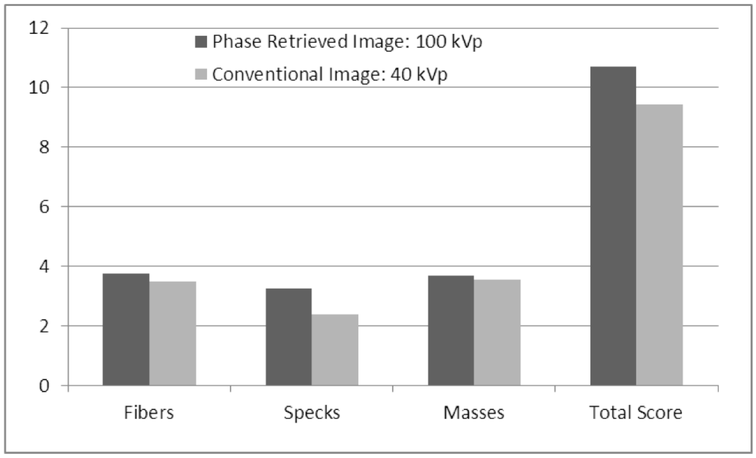

Fig. 3.
Comparison of ACR scores for the high energy phase contrast and low energy conventional images of the ACR phantom.

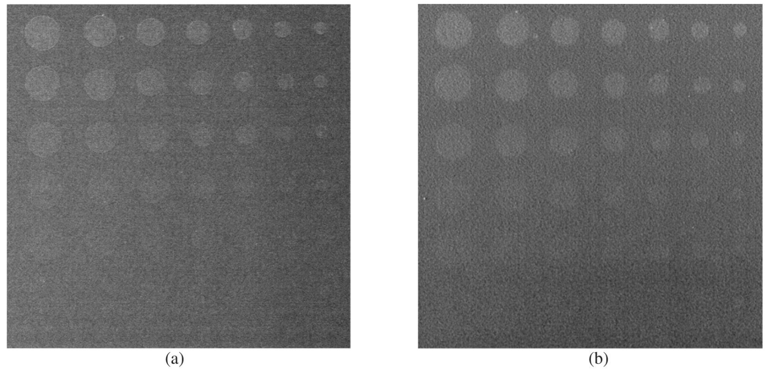

Fig. 4.
Comparison of contrast-detail phantom images, which were acquired under the following experimental settings: (a) 100 kV, 100 μA and 72 s in phase contrast mode, and (b) 40 kV, 250 μA and 192 s in conventional mode.

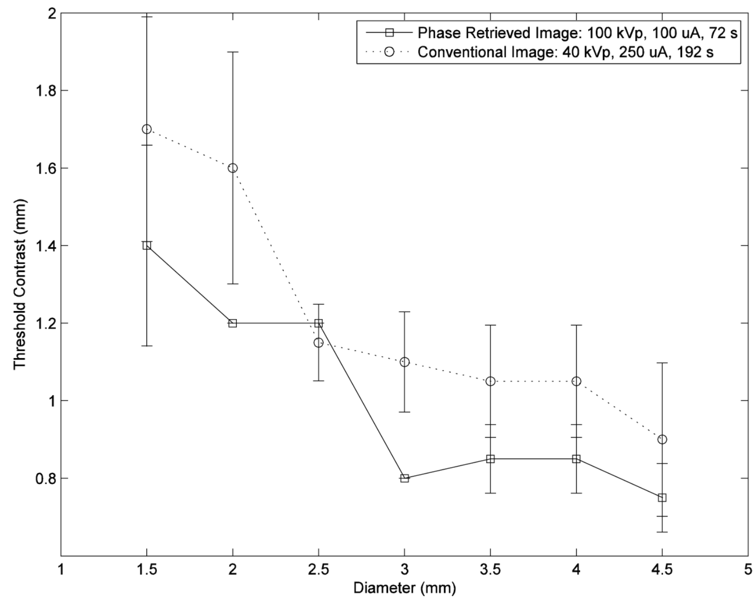

Fig. 5.

Comparison of contrast-detail curves generated from the high energy phase contrast and low energy conventional phantom images.

NIH-PA Author Manuscript

NIH-PA Author Manuscript

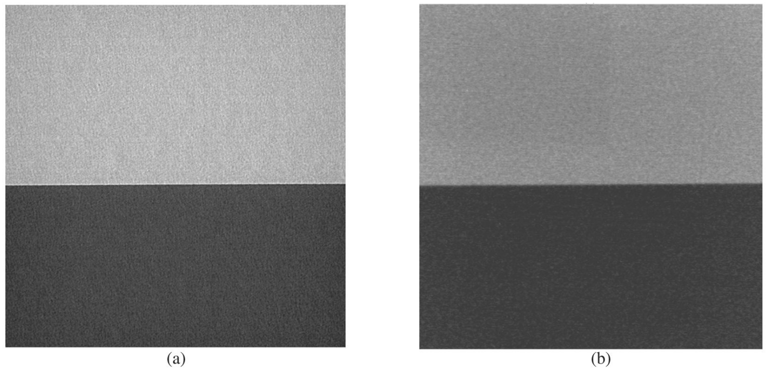

Fig. 6.
Comparison of acrylic edge phantom images, which were acquired under the following experimental settings: (a) 100 kV, 100 μA and 72 s in phase contrast mode, and (b) 40 kV, 250 μA and 192 s in conventional mode.

NIH-PA Author Manuscript
NIH-PA Author Manuscript

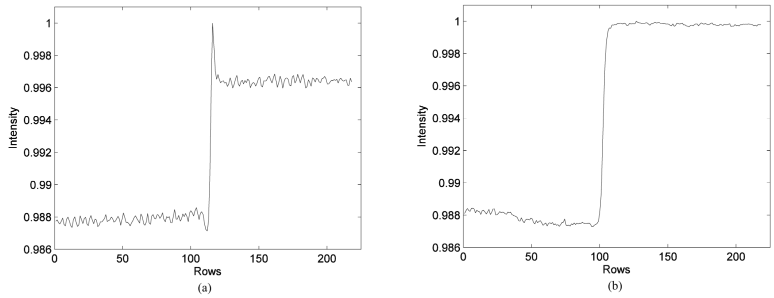

Fig. 7.

Comparison of edge profiles corresponding to the acrylic edge phantom images acquired under the following experimental settings: (a) 100 kV, 100 μA and 72 s in phase contrast mode, and (b) 40 kV, 250 μA and 192 s in conventional mode.

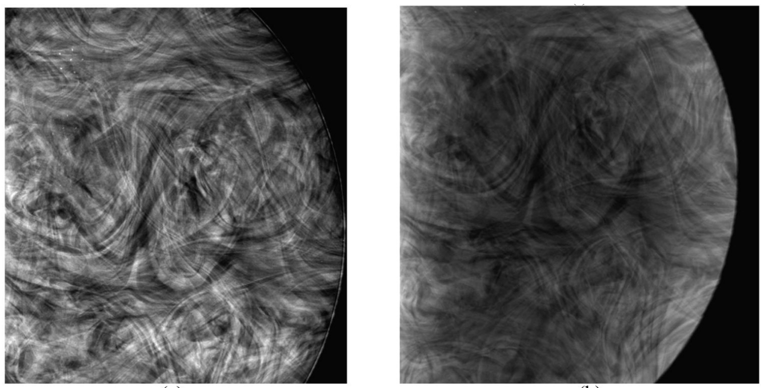

(a) (b)

Fig. 8.

Comparison of tissue-equivalent phantom images, which were acquired under the following experimental settings: (a) 100 kV, 100 μA and 72 s in phase contrast mode, and (b) 40 kV, 250 μA and 192 s in conventional mode.

Table 1

Average glandular dose calculation values for the modes compared in this study. A target D_g value was selected, and the exposure times were determined separately for each mode in order to deliver the corresponding absorbed dose.

Mode	Exposure time (s)	X_{ESE} (R)	D_{gN} (mrad/R)	D_g (mrad)
40 kV conventional	192	1.64	122.0	200.08
100 kV phase contrast	72	0.632	320.2	202.37